14èmes Journées de l'Hydrodynamique

18-19-20 novembre 2014

DGA Techniques hydrodynamiques
Chaussée du Vexin
27105 Val de Reuil

EFFET DE L'AMORTISSEMENT AERODYNAMIQUE SUR LA TENUE A LA MER D'UNE EOLIENNE FLOTTANTE A AXE VERTICAL

AERODYNAMIC DAMPING EFFECT ON THE MOTIONS OF A VERTICAL-AXIS FLOATING WIND TURBINE

R. ANTONUTTI[abc]*, N. RELUN[a], C. PEYRARD[ab]

a) EDF R&D - Electricité de France Research and Development
6 quai Watier, 78400 Chatou, France
b) Saint-Venant Hydraulics Laboratory
Université Paris-Est, 6 quai Watier, 78400 Chatou, France
c) Industrial Doctoral Centre for Offshore Renewable Energy
The University of Edinburgh, King's Buildings, Edinburgh EH9 3JL, UK
* *raffaello-externe.antonutti* [at] *edf.fr*

Résumé

L'éolien flottant est un secteur prometteur dans le domaine de l'éolien en mer, spécialement en raison du coût élevé de l'éolien posé au-delà de 50 m de profondeur. Toutefois, les défis techno-économiques présentés par cette solution requièrent des ruptures par rapport à l'éolien conventionnel ; l'une des opportunités est l'utilisation des turbines à axe vertical, qui permettraient des gains en termes de taille du flotteur et d'accès à la nacelle pour la maintenance. La modélisation du comportement d'une telle éolienne sous sollicitation de vent et de vagues nécessite une simulation aéro-hydrodynamique couplée. L'étude présentée utilise CALHYPSO, le simulateur couplé d'EDF R&D, pour l'analyse du phénomène d'amortissement aérodynamique, qui est détaillé pour le mouvement de tangage d'un concept d'éolienne flottante. Elle montre que cet amortissement compte pour 2% à 4% de l'amortissement critique, selon les conditions opérationnelles, réduisant l'amplitude de la réponse au pic de 25% à 50%.

Summary

Floating wind power represents a promising area of offshore wind in that classic bottom-fixed turbines cannot be economically installed beyond water depths of about 50 m. However, the significant challenges posed by this arrangement likely require technological breakthroughs ; one of the sought paths is to exploit the vertical axis turbine

type in order to obtain gains in floater material efficiency and nacelle maintenance access. Coupled aero-hydrodynamic simulation is required to characterise the dynamic behaviour of such a machine under the action of wind and waves. This study employs CALHYPSO, EDF R&D's floating wind turbine coupled simulator, to analyse the aerodynamic damping phenomenon impacting the pitch motion of a floating wind turbine concept. It is shown how damping depends on the rotor's operating conditions, amounting to 2% - 4% of critical and providing a 25% to 50% reduction in peak response.

I – Introduction

Floating wind power holds the potential to unlock vast offshore wind resources otherwise unavailable due to techno-economical limits : it is estimated that beyond depths of about 50-60 m bottom-fixed substructures become less attractive than floating arrangements [8]. This consideration currently drives significant R&D efforts worldwide, while leading players move on from prototype deployment to small array projects. Nevertheless, the industry is set to face considerable challenges due to the need to improve cost-effectiveness and reliability of floating wind after the proof of concept is delivered. Relatively radical innovations are thus attempted, one of these being reviving vertical-axis rotor technology. Utility-scale vertical-axis wind turbine (VAWT) R&D has been fostered by this new possible application after decades of minor attention, chiefly because of the lower nacelle, reduced number of moving parts, and tolerance to skewed flow of a VAWT compared to its horizontal-axis counterpart.
The EDF Group has engaged in a pre-commercial programme with VAWT technology developer Nénuphar and several other players, aimed at deploying a full-scale demonstrator and then a first floating windfarm off Fos-sur-Mer in the French Côte d'Azur (cf. [3]). The concurring R&D initiative led to development of in-house capabilities for the coupled mechanical analysis of floating wind turbines (FWT). Reliable design and verification of a FWT requires simulating rather complex dynamics : in principle one is dealing with a highly-dynamic, highly nonlinear system where a deformable structure is subjected to simultaneous aero-hydrodynamic loading. While resolution of the full fluid-structure interaction is indeed required to assess local loading patterns, at the concept stage a key task is characterising the global response of the FWT for a large number of loading cases. This is where engineering-level coupled dynamic models are used, that can simulate the turbine's dynamic behaviour while keeping computational cost contained.
Substantial research has addressed the effects of rotor forces on the coupled dynamic response of horizontal-axis FWTs, where the rotor control strategy is a key variable determining aerodynamic damping (cf. [9]). The coupled dynamic behaviour of floating VAWTs has also been studied, albeit to a lesser extent : examples are found in [2, 12, 16, 4, 5, 1, 15]. In this study we concentrate on the aerodynamic damping impacting the motions of an operating, floating VAWT (outlined in Figure 1, left). EDF R&D's time-domain modelling tool CALHYPSO is introduced in the methodology section, as well as the strategies adopted to extract damping and motion response information from the simulation outputs. The following section briefly describes the FWT concept employed as a case study. A range of numerical decay tests is then presented, followed by simulations in regular waves. The observed aerodynamic damping effects are then discussed, leading to a conclusive section.

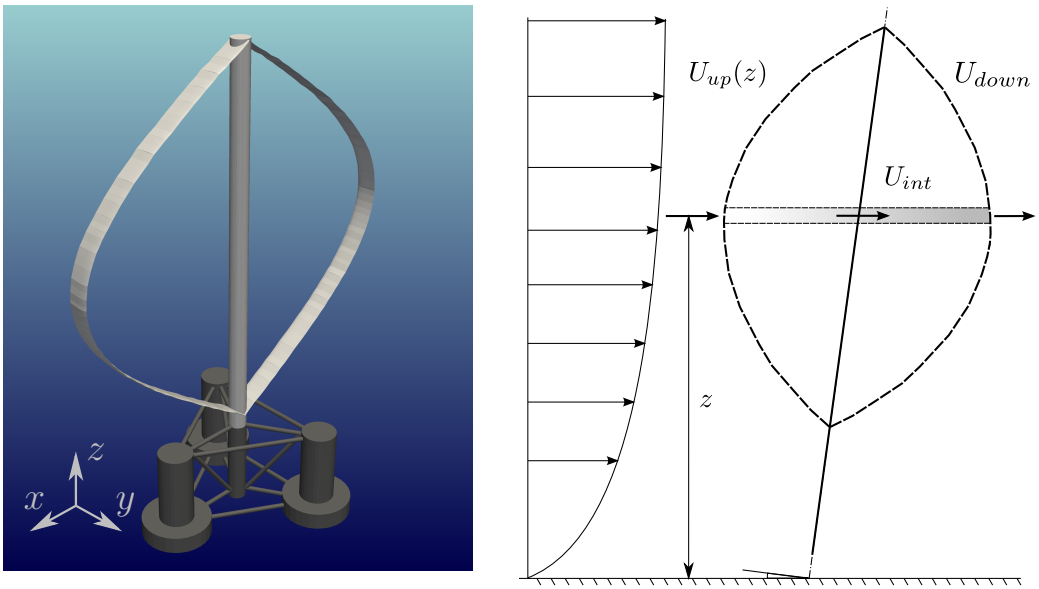

Figure 1 – Floating VAWT concept (left) and streamtube in tilted operation (right).

II – Methodology

This section outlines the approaches underpinning the current study, including aerodynamic, hydrostatic, hydrodynamic, and mooring system modelling. Also described are the key post-processing choices.

II – 1 Dynamic simulation

EDF R&D is currently developing a coupled FWT simulation software, CALHYPSO (CALcul HYdrodynamique Pour les Structures Offshore), capable of integrating the met-ocean loads exerted on the operating turbine and its substructures into a six-DoF, time-domain dynamic model based on the classic sea-keeping approach. The modelling approaches used for this study are summarised next.

Aerodynamics. The representation of aerodynamic forces is based on Paraschivoiu's double-multiple streamtube (DMST) method [13], which utilises blade element theory in combination with a two-stage momentum loss formulation. This model relies on empirical lift and drag coefficients, function of the Reynolds number and of the angle of attack, and does not resolve the aerodynamic flow explicitly. A distribution of streamtubes covers the area swept by the rotor, allowing to calculate local induction in the time domain. Dynamic stall is implemented via the Gormont model, employing Berg's correction, and the tower wake is modelled via a downstream speed deficit formulation. Not represented are rotor deformability, streamtube expansion, and dynamic inflow. The model has been verified for the studied VAWT in bottom-fixed configuration against published results (Figure 2, left). Application of DMST to a floating turbine requires inclusion of the local wind velocity and direction perturbations caused by six-DoF motion. Wind skew is treated by continuously updating the links between upstream and downstream streamtube cells as

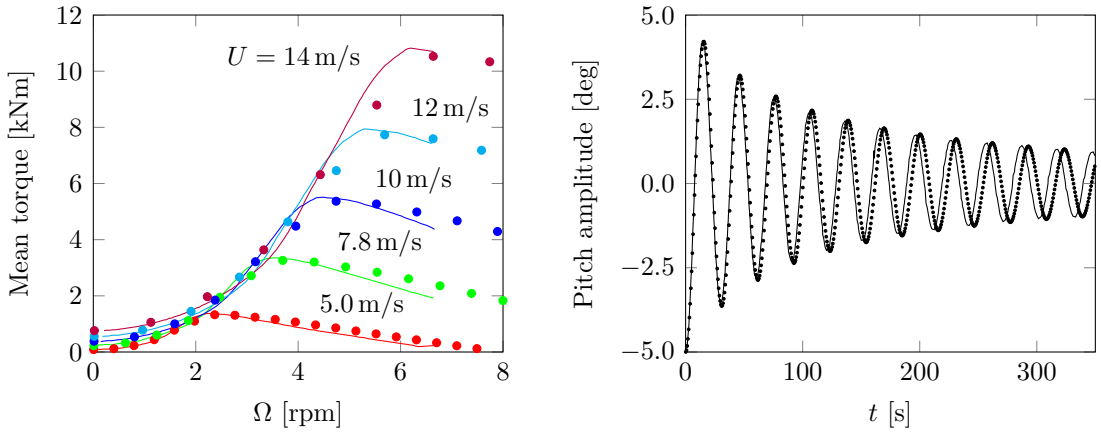

Figure 2 – Verification of the output torque of the 5 MW Darreius turbine (left) and of the floating system's pitch motion decay with $U = \Omega = 0$ (right). Dots represent the outputs of CALHYPSO and lines those of the comparable model Simo-Riflex-DMS [16, 2].

displayed in Figure 1 (right). Also, the local incident airspeed is corrected to reflect the perturbations due to platform oscillations.

Rotordynamics and control. Gyroscopic forces are included in the model with a lump-mass representation expressed in the floating system of reference. Although a proportional integral-derivative control model is available in CALHYPSO, constant rotational speed is utilised in the current study for simplicity.

Hydrostatics and hydrodynamics. Hydrostatic restoring forces are fully linearised using the conventional naval architecture approach. Potential hydrodynamic forces are obtained in the frequency domain using NEMOH, a linear diffraction-radiation solver developed by École Centrale de Nantes [7]. Conversion to the time domain is achieved via the impulsive method introduced by [6]. Drag forces exerted by the fluid on the hull components are evaluated using the local relative flow speed obtained by combining structure motion and incident wave motion. The speed vector is then decomposed into an axial and a transverse component and the corresponding drag forces are computed. The dominating viscous phenomenon is flow separation about the lower columns, where an axial drag coefficient of 4.80 is applied, justified by the basin tests described in [11]. The comparison between the time-domain pitch decay motion of the studied FWT as calculated by CALHYPSO and by an alternative software is shown in Figure 2 (right).

Moorings model. Since station-keeping of the studied FWT is achieved with a catenary mooring system, its restoring behaviour becomes markedly nonlinear when the structure undergoes large offsets, most notably under the action of wind thrust. This calls for the use of a nonlinear approach, such as the position-updated quasi-static method. Although this is available in CALHYPSO, in the present study a fully linearised model is adopted to avoid changes in effective mooring stiffness following the application

of wind thrust. This would in turn alter the natural periods of the structure, making it more difficult to compare motion extinction with and without incident wind.

Motion resolution. All active and reactive forces, with the exception of the rigid structure's own inertial forces, are assembled into the right hand side term of the six-DoF equations of motion, allowing to compute the acceleration vector. This is integrated twice in the time domain to reconstruct the motion history with a Runge-Kutta 4^{th} order scheme.

II – 2 Post-processing

Elimination of 2P harmonic. When a symmetric, two-bladed turbine is operating, the motion outputs of any dynamic simulation contain a periodic fluctuation of period $T_{2\text{P}}$, that equals a half of the rotor's revolution period. This effect is particularly marked for a Darreius VAWT because of the large force swings involved, and implies that output data must be post-processed in order to retrieve certain sets of information. In this study FWT motion is characterised *after* having filtered out the aforementioned fluctuation. In the case of decay tests, a moving average approach is employed to smoothen the signal and retrieve the appropriate oscillation peak amplitudes for computation of the damping ratio. For what concerns motion under regular waves, pseudo-RAOs are retrieved from steady-state motion using the amplitude of the Fourier component which corresponds to wave forcing. These two processes are depicted in Figure 3.

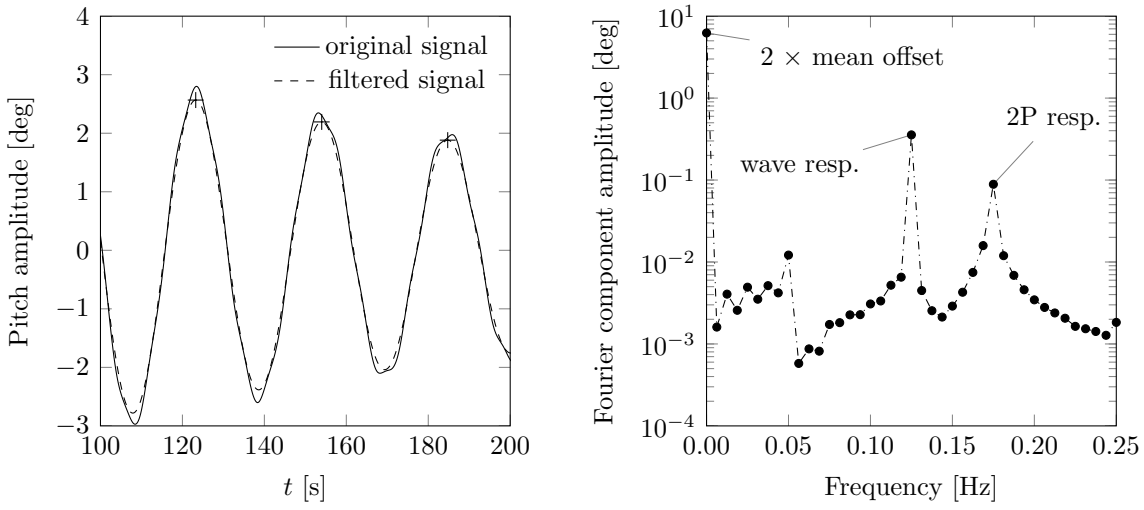

Figure 3 – Filtering of 2P component from the pitch decay signal (left) and Fourier transform of the steady-state pitch response in waves (right).

Evaluation of damping ratio. When numerical decay tests are carried out, filtering the 2P motion component leaves a decaying, oscillating signal whose peaks are denoted $\hat{x}_{\text{i}}$. Positive linear damping in underdamped dynamic systems results in exponentially

decaying, sinusoidal free oscillations. Although the system in question contains significant nonlinearities and hence motion extinction does not exactly assume this form, it is nevertheless possible to evaluate the equivalent linear damping ratio ζ for any number of oscillation cycles N with

$$2\pi N\zeta = \log\left(\frac{\hat{x}_{\mathrm{i}}}{\hat{x}_{\mathrm{i}+N}}\right) . \tag{1}$$

By imposing $N = 1$ in Equation 1, the equivalent damping ratio for each oscillation cycle is obtained. This is the quantity ultimately used to characterise the aerodynamic damping affecting the free oscillations of a floating VAWT.

III – Floating wind turbine concept

The floating VAWT concept used for this study, shown in Figure 1 (left), has been proposed by [16] and further characterised in [2]. It consists in a combination of a 5 MW Darreius-troposkein turbine developed by [15] for floating applications and the OC4-DeepCwind semi-submersible support structure detailed in [14]. As previously said, this concept uses catenary mooring lines for station-keeping : its particulars are available in [14], as well as the values of the corresponding linearised restoring coefficients. The principal turbine properties, floater geometric parameters, and FWT mass/inertia characteristics are given in Table 1.

Table 1 – Properties of floating VAWT concept. Mooring weight is included with an equivalent lump mass. Inertias are expressed with respect to the origin O at the SWL.

Turbine geometry		**Floater geometry**	
Rotor radius [m]	63.74	Design draft [m]	20.0
Rotor height [m]	129.56	Hull volume at design draft [m^3]	13919
Airfoil type	NACA 0018	Column centre-to-centre spacing [m]	50.0
Blade chord [m]	7.45	Diameter of central column [m]	6.5
Turbine operation		Diameter of upper offset column	12.0
Rated power [MW]	5.0	Diameter of lower offset column [m]	24.0
Rated rotor speed [rpm]	5.26	Height of lower offset column [m]	6.0
Rated wind speed [m/s]	14.0	Bracing diameter [m]	1.6
Global mass and inertia			
Displacement [t]	14267	Roll/pitch moment of inertia [$t\,m^2$]	$1.500 \cdot 10^{10}$
Height of CoG from keel [m]	11.27	Yaw moment of inertia [$t\,m^2$]	$1.262 \cdot 10^{10}$

IV – Results

This section reports the key outcomes of the time-domain simulations. Motion decay is presented in terms of evolution of the single-cycle damping ratio over time. Pitch response in waves is supplied in the form of pseudo-transfer functions. In all cases a baseline operating condition is defined where rotor and wind speed respectively equate $\Omega = 5.217\,\mathrm{rpm}$ and $U = 14.00\,\mathrm{m/s}$. A set of operating points is also generated around the above pairing by perturbing in turn Ω and U. Incident wind is considered stationary, and its vertical profile constant.

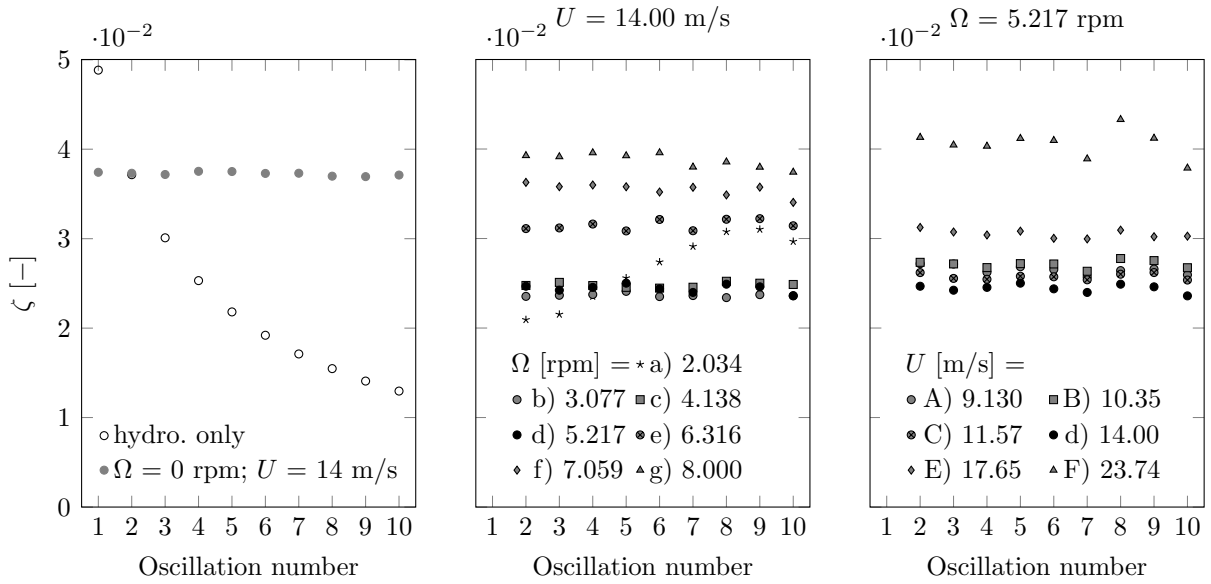

Figure 4 – Damping ratio ζ of pitch oscillations with hydrodynamics only and parked rotor (left), varying rotor speed (centre), and varying incident wind speed (right).

IV – 1 Decay tests

Pitch motion decay about the mean equilibrium position is obtained for a range of operating conditions. Due to significant inter-DoF coupling, it is chosen to allow the structure to oscillate in pitch only - otherwise the observed dissipation would be associated to concurring multi-DoF mechanisms rather than pitch alone. In order to isolate the damping originating from rotor forces, all sources of hydrodynamic damping are zeroed ; the only exception is the hydrodynamically damped case, reported for comparison, where rotor forces are suppressed instead.

All tests are set up by applying a pitch displacement of $+5\,\text{deg}$ at $t = 0\,\text{s}$ from the mean offset attained with the rotor in operation, before releasing the structure into a free oscillation regime. The incident wind propagates along the x axis. Application of Equation 1, with $N = 1$, to the first ten motion cycles leads to the results of Figure 4. The first cycle does not appear where a moving average is used (i. e. for $\Omega \neq 0\,\text{rpm}$). In the 'hydrodynamics only' case, damping decays over time : this reflects its quadratic nature, caused by the dominance of drag-type forces ; at the natural period of pitch, $T_\text{p} \approx 31\,\text{s}$, linear radiation damping is close to nil. The observed aerodynamic damping ratios vary between 2% and 4%, and keep nearly constant over time. This reveals that the system is almost linearly damped, a feature that will be justified in the discussion section. It can be noted that in the 'parked rotor' configuration of Figure 4 (left) all damping descends from the action of aerodynamic drag forces : the rotor's azimuth is constant and corresponds to that shown in Figure 1 (left), implying that the flow is perpendicular to the chord of all blade elements. As it will be discussed, the resulting damping ratio is also constant over time in virtue of the presence of a relatively large incident wind speed U.

There is one exception to the above statement on nearly-constant aerodynamic damping,

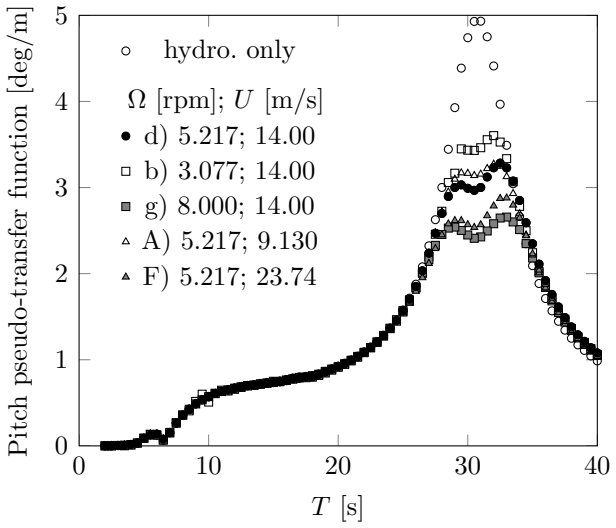

Figure 5 – Pseudo-transfer function of pitch for different operating conditions.

which is case a) : the oscillation of ζ observed in Figure 4 (centre) is explained by the excitation of pitch resonant motion by the 2P aerodynamic load, with $T_\mathrm{p}/T_\mathrm{2P} \approx 2.09$. In this particular case, inferring damping from peak amplitude decay is incorrect.

IV – 2 Motion in regular waves

Incident regular waves propagating along positive x (collinear with the wind) are used here to excite the system, which is free to move in the six DoF. Only pitch motion is analysed, which is presented in the frequency domain through pseudo-transfer functions. These are obtained by normalising the amplitude of the motion's Fourier component of choice over the incident wave amplitude, $H/2$, where $H = 2\,\mathrm{m}$ is the wave height. The frequency of this component is equal to the wave frequency.

Figure 5 displays pitch response for a subset of the operating conditions presented in IV – 1. When the turbine is operating, significant aerodynamic damping of pitch around the resonance peak is observed. In the case of the studied FWT concept, this is far removed from the prevalent 1$^\mathrm{st}$ order wave force band, hence variations in resonant motion amplitude due to varying damping bear a relatively minor impact on the turbine's motion in waves. Nevertheless this may not be the case for response characteristics in different degrees of freedom (e. g. horizontal, where higher-order loads can cause large resonant motions), and in general for floating systems whose natural periods are closer to the wave band.

With respect to the hydrodynamics-only case, the peak amplitude of pitch is reduced by 25% to 50% thanks to the presence of rotor forces. The differences in peak height across operating cases reflect the amounts of aerodynamic damping at play and are in general agreement with the values of ζ shown in Figure 4. However, minor apparent inconsistencies manifest, such as the larger resonant motion damping of case g) compared to case F). These, along with the undulating shape of the peaks, are due to significant roll-pitch coupling arising from the rotor gyroscopic effect, that causes roll motion to increasingly participate in dissipation when rotor speed and/or motion is large.

V – Discussion

In this section the simulation outcomes are subjected to a more in-depth analysis aiming at reconciling the observed trends with the underlying physical phenomena and the corresponding modelling approaches.

V – 1 Quasi-linearity of aerodynamic damping

As pointed out in IV – 1, the nearly constant value of ζ characterising the free pitch oscillations for a given operating condition is a manifestation of aerodynamic damping force linearity. In the model all aerodynamic forces acting on the blades are computed with the classic lift and drag formulation ; although both of these quantities are a quadratic function of the airspeed, they become essentially linear with respect to its perturbations as explained next.
The magnitude of the drag force exerted on an object in presence of an unperturbed, constant airflow of speed U can be written in the following general form, assumed that the object oscillates with instantaneous velocity $\dot{x}$ in the same direction as U :

$$D = \frac{1}{2}\rho A C_D \left(U - \dot{x}\right)^2 = \frac{1}{2}\rho A C_D \left(U^2 + \dot{x}^2 - 2U\dot{x}\right) . \tag{2}$$

It is hence possible to express the instantaneous damping coefficient of motion in the x direction from Equation 2 with

$$-\frac{\partial D}{\partial \dot{x}} = \rho A C_D \left(U - \dot{x}\right) \approx \rho A C_D U . \tag{3}$$

It can be calculated that at most rotor stations the local velocity $\dot{x}$ induced by pitch oscillations (at the natural period T_p, with an amplitude of a few degrees) is at least one order of magnitude smaller than U, given that U is in the order of 10 m/s. This justifies the approximation in Equation 3. It is found that the dominant component of the drag-induced damping coefficient is $\dot{x}$-independent, implying linearity of drag damping for large enough values of $U/\dot{x}$.
At dead up-wind blade passage, within the region where large part of the aerodynamic forcing is generally produced, the quasi-steady lift force arising on a blade element oscillating with instantaneous speed $\dot{x}$ in the direction of the incident wind (cf. Figure 6, left) can be written as

$$L = \frac{1}{2}\rho A \left.\frac{dC_L}{d\alpha}\right|_{\alpha=0} \arctan\left[\frac{U_\mathrm{up}\left(1-a\right) - \dot{x}}{\Omega r}\right] \left\{\left[U_\mathrm{up}\left(1-a\right) - \dot{x}\right]^2 + \Omega^2 r^2\right\} , \tag{4}$$

where a is the local axial induction factor and r the blade element radius. A linear $C_L\left(\alpha\right)$ relationship is assumed ; as shown in Figure 6 (right), for a NACA 0018 profile this approximation is accurate for $\alpha \in [-10, 10]$ deg. By considering that this limitation translates into $\left[U_\mathrm{up}\left(1-a\right) - \dot{x}\right]/\Omega r \lessapprox 0.2$, and by introducing the small angle approximation, the lift force can be re-expressed with

$$L \approx \frac{1}{2}\rho A \left.\frac{dC_L}{d\alpha}\right|_{\alpha=0} \left[U_\mathrm{up}\left(1-a\right) - \dot{x}\right] \Omega r . \tag{5}$$

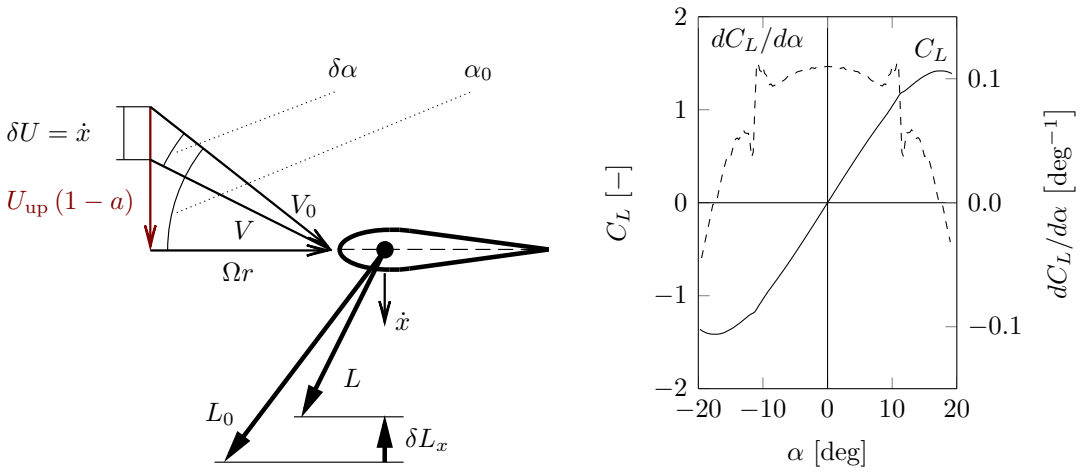

Figure 6 – Lift-induced damping mechanism (left) and lift coefficient characteristic of a NACA 0018 airfoil at high Re with its first derivative (right).

Assuming $L_x \approx L$, where L_x is the component of the lift force that is aligned with the airfoil oscillation, which holds for small angles of attack, allows to write an approximated expression of the instantaneous lift-induced damping coefficient in the x direction :

$$-\frac{\partial L_x}{\partial \dot{x}} \approx \frac{1}{2}\rho A \left.\frac{dC_L}{d\alpha}\right|_{\alpha=0} \Omega r\,. \tag{6}$$

It can be noted that the above coefficient is proportional to the rotor speed. Another way to look at this mechanism is focussing on the δL_x lift component generated by the airspeed perturbation shown in Figure 6 (left) : in the absence of blade oscillations, the combination of the relative airspeed components due to the element's tangential speed Ωr and to the transverse wind speed $U_{\text{up}}\,(1-a)$ forms the local incident airspeed vector V_0. An oscillation-induced velocity perturbation, $\dot{x}$, causes it to be redefined as V, a vector with different magnitude and, most importantly, different angle of attack over the profile, $\alpha = \alpha_0 - \delta\alpha$. This causes a change in lift force which gives rise to an extra component δL_x that is opposed to $\dot{x}$ for small angles of attack.
The key information emerging from the damping coefficient examples of Equations 3 and 6 is that i) lift and drag forces apply approximately linear damping in the x direction at the upwind (and downwind) blade passage and ii) the drag-induced damping coefficient is proportional to U whilst the lift-induced coefficient is proportional to Ω.

V – 2 Aerodynamic damping dependencies

The results presented in IV – 1 and IV – 2 suggest that the aerodynamic damping of pitch motion significantly depends on the turbine's operating parameters, namely rotor speed and incident wind speed (direction also matters, which is not treated here). Rearranging the results in terms of tip-speed ratio (TSR) can help in understanding the underlying patterns. This is accomplished by extracting the values of ζ corresponding to the 2$^{\text{nd}}$ pitch oscillation from the curves shown in Figure 4. These values are displayed

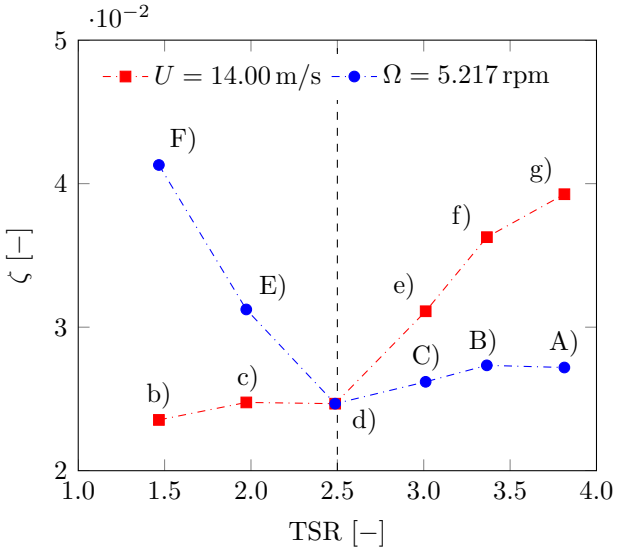

Figure 7 – Damping ratio of second pitch oscillation for varying tip-speed ratios.

as a function of TSR in Figure 7. The most striking feature of this graph is that for TSR < 2.5 the main parameter influencing ζ is wind speed, with ζ positive function of U, whilst damping is relatively insensitive to changes of rotational speed. Conversely, for TSR > 2.5 it is the rotational speed that mostly influences the damping ratio. In the light of what has been shown in V – 1, the dependence of damping on U can be associated to the drag mechanism, whilst where damping is most affected by Ω the variations can be mainly attributed to lift forces. This identifies a critical TSR ≈ 2.5 where a shift occurs between a drag-dominated and a lift-dominated regime.

In support of this interpretation, Figure 8 shows the distribution of the angles of attack over a 360 deg blade sweep for three selected operating conditions, using a bottom-fixed turbine. Any datum with $|\alpha| \leq 10\,\mathrm{deg}$ is coloured in green. This denotes attached flow in the linear region of $C_L(\alpha)$. The green-white-red transition defines local angles of attack with $|\alpha| \in]10, 17.5[\,\mathrm{deg}$, where the flow is attached and the slope of the $C_L(\alpha)$ function is generally declining. $|\alpha| = 17.5\,\mathrm{deg}$ is defined as the critical angle of attack for which C_L reaches its maximum (cf. Figure 6, right). Beyond this point - the red areas in the figure - stall occurs and the airfoil is no longer capable of reacting to an increase in angle of attack with an increase in lift force. The lift-induced damping mechanism breaks.

The azimuth regions generating most aerodynamic damping in pitch are upwind and downwind, respectively to the left and to the right of the sweep plots of Figure 8. In the subcritical operating condition b) the blades are stalled over most of the upwind and downwind sweeps. This in turn implies that the lift-based damping mechanism is marginal, and that aerodynamic damping in pitch mainly arises from U-dependent drag (affecting both blades and tower). In the transcritical case d) part of the upwind & downwind sweep occurs in attached flow regime and part is stalled. Finally, the supercritical operating condition f) is characterised by mostly attached flow over a blade sweep : here the Ω-dependent lift mechanism becomes most important in determining aerodynamic damping.

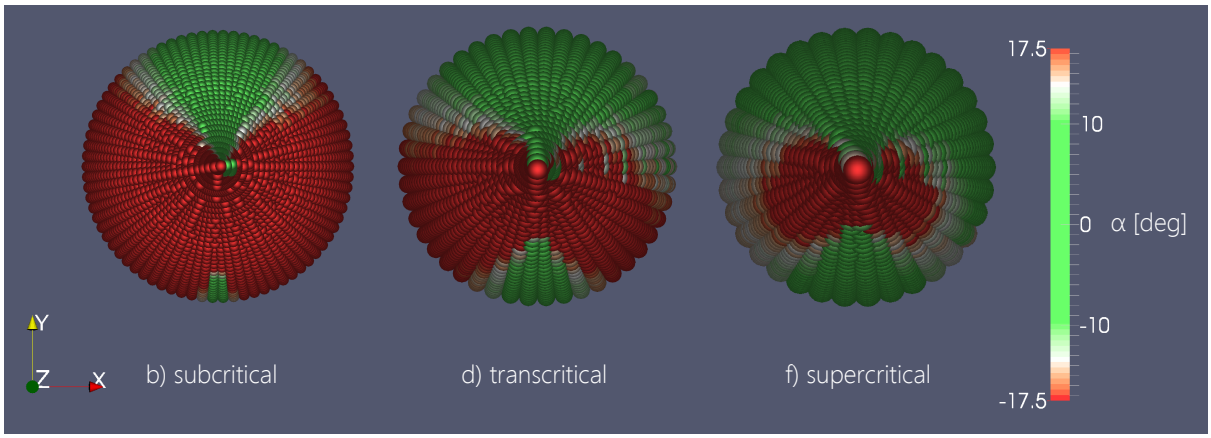

Figure 8 – Top-down view of airfoil angles of attack for all blade azimuths.

VI – Conclusion

This study characterises the aerodynamic damping of a floating VAWT affecting its pitch motion in waves. It exploits the results of a set of dynamic simulations carried out with EDF R&D's coupled dynamics software CALHYPSO. Special attention is needed in post-treating the motion outputs because of the presence of a significant 2P response component. Decay simulations in particular must be handled with caution since one deals with 'excited' motion extinction : spurious phenomena can occur, such as resonance, which invalidate the common procedure for calculation of the damping ratio.
The aerodynamic damping in pitch supplied by the operating rotor is found to depend on both incident wind speed and rotor speed. It amounts to about 2% - 4% of the critical damping and provides a reduction in peak pitch response of 25% to 50%. The damping ratios emerging from the decay simulations are consistent with the results of the dynamic simulations in regular waves, and their dependencies reveal the contribution of both lift- and drag-induced damping mechanisms. These mechanisms are shown to function in an essentially linear fashion, a finding that is consistent with the experimentally observed behaviour of a floating HAWT [10]. Analysing the evolution of the damping ratio with respect to the tip-speed ratio indicates that it exists a critical TSR below which the drag mechanism dominates the variations in damping, while lift forces explain the variations occurring above the critical TSR.
It is important to remark that these results and interpretations do not necessarily represent the physics of a real FWT system, but rather the behaviour of a numerical model that is widely used across the industry. The aerodynamic model in particular does not give account of rotor wake dynamics, which are expected to affect rotor loads especially in the high TSR region. Moreover, the non-stationarity due to platform motion is treated under the hypothesis that it only constitutes a weak perturbation to streamtube equilibrium. Further numerical, and possibly experimental investigation on the aerodynamic damping of floating VAWTs is thus required to verify and validate the shown phenomena.

VII – Acknowledgements

IDCORE is funded by the ETI and the RCUK Energy programme, grant number EP/J500847/1. The authors are grateful for the funding provided by these institutions, and to EDF R&D for hosting and supervising the industrial doctorate.

References

[1] P. Blusseau and M. H. Patel. Gyroscopic effects on a large vertical axis wind turbine mounted on a floating structure. *Renewable Energy*, 46 :31–42, 2012.

[2] M. Borg, K. Wang, M. Collu, and T. Moan. A comparison of two coupled models of dynamics for offshore floating vertical axis wind turbines. In *Proc. 33rd International Conference on Ocean, Offshore and Arctic Engineering*, San Francisco, CA, USA, 2014.

[3] M. Cahay, E. Luquiau, C. Smadja, and F. Silvert. Use of a vertical wind turbine in an offshore floating wind farm. In *Proc. Offshore Technology Conference 2011*, Houston, TX, USA, 2011.

[4] M. Collu, M. Borg, A. Shires, and F. P. Brennan. FloVAWT : Progress on the development of a coupled model of dynamics for floating offshore vertical axis wind turbines. In *Proc. 32nd International Conference on Ocean, Offshore and Arctic Engineering*, Nantes, France, 2013.

[5] M. Collu, M. Borg, A. Shires, F. N. Rizzo, and E. Lupi. FloVAWT : Further progresses on the development of a coupled model of dynamics for floating offshore VAWTs. In *Proc. 33rd International Conference on Ocean, Offshore and Arctic Engineering*, San Francisco, CA, USA, 2014.

[6] W. E. Cummins. The impulse response function and ship motions. Technical Report Report 1661, David Taylor Model Basin, 1962.

[7] Ecole Centrale de Nantes. LHEEA - NEMOH. Online : http ://lheea.ec-nantes.fr/doku.php/emo/nemoh/start. Accessed : June 2014.

[8] EWEA. Deep water - the next step for offshore wind energy. Technical report, European Wind Energy Association, 2013.

[9] J. M. Jonkman. Influence of control on the pitch damping of a floating wind turbine. Technical Report NREL/CP-500-42589, National Renewable Energy Laboratory, 2008.

[10] M. Le Boulluec, J. Ohana, A. Martin, and A. Houmard. Tank testing of a new concept of floating offshore wind turbine. In *Proc. 32nd International Conference on Ocean, Offshore and Arctic Engineering*, Nantes, France, 2013.

[11] M. Masciola, A. Robertson, J. Jonkman, A. Coulling, and A. Goupee. Assessment of the importance of mooring dynamics on the global response of the DeepCwind floating semisubmersible offshore wind turbine. In *Proc. 23rd International Offshore and Polar Engineering Conference*, Anchorage, AK, USA, 2013.

[12] K. O. Merz. A method for analysis of VAWT aerodynamic loads under turbulent wind and platform motion. *Energy Procedia*, 24 :44–51, 2012.

[13] I. Paraschivoiu. *Wind Turbine Design : With Emphasis on Darrieus Concept*. Polytechnic International Press, Montréal, Canada, 2002.

[14] A. Robertson, J. Jonkman, M. Masciola, and H. Song. Definition of the semisubmersible floating system for phase II of OC4. Technical Report NREL/TP-5000-60601, National Renewable Energy Laboratory, 2014.

[15] L. Vita. *Offshore Floating Vertical Axis Wind Turbines with Rotating Platform*. PhD thesis, Risø DTU, Roskilde, Denmark, 2011.

[16] K. Wang, T. Moan, and M. O. L. Hansen. A method for modeling of floating vertical axis wind turbine. In *Proc. 32nd International Conference on Ocean, Offshore and Arctic Engineering*, Nantes, France, 2013.